Soft Matter

Cite this: *Soft Matter*, 2011, **7**, 7094

www.rsc.org/softmatter

PAPER

Structural changes in block copolymer micelles induced by cosolvent mixtures†

Elizabeth G. Kelley,‡[a] Thomas P. Smart,‡[a] Andrew J. Jackson,[ab] Millicent O. Sullivan[a] and Thomas H. Epps, III*[a]

Received 24th March 2011, Accepted 23rd May 2011
DOI: 10.1039/c1sm05506b

We investigated the influence of tetrahydrofuran (THF) addition on the structure of poly(*1,2*-butadiene-*b*-ethylene oxide) [PB-PEO] micelles in aqueous solution. Our studies showed that while the micelles remained starlike, the micelle core-corona interfacial tension and micelle size decreased upon THF addition. The detailed effects of the reduction in interfacial tension were probed using contrast variations in small angle neutron scattering (SANS) experiments. At low THF contents (high interfacial tensions), the SANS data were fit to a micelle form factor that incorporated a radial density distribution of corona chains to account for the starlike micelle profile. However, at higher THF contents (low interfacial tensions), the presence of free chains in solution affected the scattering at high q and required the implementation of a linear combination of micelle and Gaussian coil form factors. These SANS data fits indicated that the reduction in interfacial tension led to broadening of the core-corona interface, which increased the PB chain solvent accessibility at intermediate THF solvent fractions. We also noted that the micelle cores swelled with increasing THF addition, suggesting that previous assumptions of the micelle core solvent content in cosolvent mixtures may not be accurate. Control over the size, corona thickness, and extent of solvent accessible PB in these micelles can be a powerful tool in the development of targeting delivery vehicles.

1. Introduction

Amphiphilic block copolymer assemblies have become increasingly important for targeted drug delivery applications due to their synthetic versatility, stability, and ability to encapsulate therapeutic molecules.[1] One key area of research focuses on manipulating ligand display on solution assembled polymeric nanostructures to enable site-specific targeting. Previous work to create targeting delivery systems has typically involved end-functionalization of the polymer chains with ligands.[2–4] However, the addition of ligands to the periphery of polymeric nanostructures often alters amphiphilic self-assembly[2,3] and evokes an immune response, leading to rapid clearance of the polymer assemblies from the body.[4] Thus, the combination of controlled self-assembly and selective accessibility of reactive groups is vital for achieving the desired ligand expression.

The solution assembly of amphiphilic block copolymers arises from a delicate balance of free energy contributions from the hydrophobic and hydrophilic blocks, as well as the interface between the two blocks.[5–8] This balance can be altered by changing the block copolymer molecular weight, the relative weight fractions of the hydrophobic and hydrophilic blocks, the chemical composition of each block, and the polymer architecture (diblock, triblock, miktoarm, *etc.*), leading to the formation of various nanostructures including micelles and vesicles.[9–11]

Although amphiphile self-assembly produces a diverse array of structures, access to this range of structures requires the synthesis of multiple polymers. Fortunately, non-synthetic methods such as the manipulation of solvent conditions can be used to control the core-corona interfacial free energy for various copolymer systems, and thereby more easily manipulate solution assembly.[6,7,12–19] For example, Eisenberg *et al.* demonstrated the reversible transition from spherical micelles to cylindrical micelles to vesicles when the solvent quality for the core block was altered using cosolvent mixtures.[15,16] Additionally, Lund *et al.* studied the effects of water/*N*,*N*-dimethylformamide (H_2O/DMF) cosolvent mixtures on poly([ethylene-*co*-propylene]-*b*-[ethylene oxide]) [PEP-PEO] spherical micelles by small angle neutron scattering (SANS).[6] They reported a decrease in micelle size with increasing DMF content due to the reduction in core-corona interfacial tension and noted that the decrease in

[a]*Department of Chemical Engineering, University of Delaware, Newark, DE, 19716, USA. E-mail: thepps@udel.edu; Fax: +1 302 831 1048; Tel: +1 302 831 0215*
[b]*NIST Center for Neutron Research, Gaithersburg, MD, 20899, USA*

† Electronic supplementary information (ESI) available: Experimental results for angle dependent light scattering of PB-PEO micelles in cosolvent mixtures, PB turbidity studies, and PEO changes in volume with solvent quality are presented in the Supplementary Information. See DOI: 10.1039/c1sm05506b

‡ These authors contributed equally to this work.

aggregation number was in good agreement with the scaling relationship for starlike micelles by Halperin.[20] While their study demonstrated the effects of interfacial tension on micelle size, they were unable to characterize the effect of interfacial tension on the core-corona interfacial profile due to minimal scattering contributions from the PEP core.

Building on the study by Lund *et al.*,[6] we have investigated the effects of interfacial tension on micelle structures, and in particular, on the core-corona interface. Theoretical and experimental studies of immiscible polymer interfaces in bulk materials have shown that decreasing the interfacial energy between the polymers broadens the interface.[21–24] Extending these studies to the solution assembly of amphiphilic block copolymers, we present the effects of interfacial tension on the core-corona interface in poly(*1,2*-butadiene-*b*-ethylene oxide) [PB-PEO] micelles. The interfacial tension was controlled using water/tetrahydrofuran (H_2O/THF) mixtures. THF and H_2O are miscible solvents, where THF is a good solvent for PB-PEO, while H_2O is selective for the PEO block. Thus, the THF content in the cosolvent mixture could be employed to manipulate the core-corona interfacial tension. By increasing the THF content and thus reducing the interfacial tension in our assembled nanostructures, we show the evolution from a sharp core-corona interface in pure H_2O,[11,25–27] to a diffuse interface at higher THF contents.

We quantified the changes in micelle composition profile primarily through contrast variations in SANS experiments and detailed SANS data modeling. By selectively deuterating the corona of the micelles, we were able to minimize scattering contributions from the corona, and characterize scattering from the micelle core and core-corona interface. Our SANS studies were complemented by small angle X-ray scattering (SAXS), dynamic light scattering (DLS), cryogenic transmission electron microscopy (cryo-TEM), and proton nuclear magnetic resonance (^{1}H NMR) spectroscopy experiments. Moreover, the experimentally determined micelle sizes were compared to theoretical scaling relationships for the dependence of micelle size on core-corona interfacial tension.

Of particular interest were the micelle structures formed at higher THF contents, where the PB chains became solvated and were revealed in the micelle corona due to the broadening of the core-corona interface. The tunable composition profile and the ability to encapsulate hydrophobic materials make these micelles interesting precursors to drug delivery vehicles. In future studies, stabilizing these solvent induced structures *via* partial cross-linking[28,29] will enable THF removal, while simultaneously maintaining the broad core-corona interface. We anticipate that the solvent accessible, pendant vinyl groups of the PB in these assemblies will enable subsequent functionalization to create targeting drug carriers with controllable ligand display.

2. Materials and methods

2.1 Materials

Ethylene oxide and *1,3*-butadiene were purchased from Sigma Aldrich. Ethylene oxide-d_4 (EO-d_4, 99.7% D), deuterium oxide (D_2O, 99.9% D), and tetrahydrofuran-d_8 (THF-d_8, 99.6% D) were purchased from Cambridge Isotopes. All other chemicals were purchased from Fisher Scientific. Monomers were purified by distillation from butylmagnesium chloride (EO and EO-d_4) or n-butyllithium (*1,3*-butadiene). THF for the polymerizations and solution preparation was degassed with argon and further purified by passage through two neutral alumina columns prior to use. Ultrapure H_2O for micelle solution preparation was obtained from a Milli-Q water purification system. D_2O and THF-d_8 were used without further purification.

PB_{57}-PEO_{183} and PB_{57}-*d*PEO_{167} [poly(butadiene-*b*-ethylene oxide-d_4)], where the subscripts denote the degree of polymerization, were synthesized by anionic polymerization using established protocols.[30] The PB-PEO and PB-*d*PEO block copolymers in this study were synthesized from the same PB parent precursor. The PB precursor (M_n = 3.2 kg mol^{-1}, PDI = 1.06, 92 ± 1% *1,2*-PB units) was characterized using gel permeation chromatography (GPC) with poly(styrene) standards, matrix-assisted laser desorption/ionization time-of-flight mass spectrometry (MALDI TOF MS),[31] and ^{1}H NMR. PB-PEO (M_n = 11.2 kg mol^{-1}, PDI = 1.03) and PB-*d*PEO (M_n = 11.1 kg mol^{-1}, PDI = 1.05) block copolymers were analyzed using GPC and ^{1}H NMR, and the diblock copolymers had hydrophilic weight fractions of 0.72 and 0.71, respectively.

2.2 Sample preparation

Micelle solutions were prepared by adding H_2O to dry polymer powder and stirring the solutions for 3 days. Next, THF was added to achieve the desired solvent composition, and the solutions were stirred for an additional 3 days before analysis. All solutions contained a final concentration of 2.4 mg mL^{-1} polymer in cosolvent solution. Solvents used to prepare the solutions were passed through a 0.2 μm filter to ensure that the samples were dust free.

2.3 Sample analysis

Contact angle. A thin film of the PB precursor (~100 nm) was prepared by flow coating a polymer solution in THF onto a silicon substrate.[32] Contact angle measurements of H_2O/THF cosolvent mixtures on the PB thin film were carried out on a First Ten Ångstroms (FTÅ) 125 contact angle measuring system. Liquid drops (3 μL) were dispensed and placed on the PB film with a Distriman pipette. Contact angle analysis was performed by using the FTÅ software and the drop shape method to determine the contact angle. Each contact angle was measured <0.5 s after each droplet first came into contact with the PB surface.[33] A minimum of five contact angles per sample were measured. The average value of these angles was used in the interfacial tension calculations. The interfacial tension (γ) between PB and the H_2O/THF mixtures was calculated from the measured contact angles according to Young's equation[19]

$$\gamma = \gamma_{PB} - \gamma_{Sol}\cos\theta \quad (1)$$

where γ_{PB} is the surface tension of PB,[34] γ_{Sol} is the surface tension of the H_2O/THF mixture,[35] and θ is the measured contact angle.

Dynamic light scattering (DLS). DLS experiments were performed using a Lexel Laser Inc. 488 nm, 100 mW laser, coupled with a Brookhaven Instruments Corporation goniometer. The

intensity auto-correlation function was recorded at angles from 20°–140° and analyzed using the CONTIN algorithm.[36] All measurements were performed at 25 °C.

Cryogenic transmission electron microscopy (cryo-TEM). Samples for cryo-TEM were prepared at 25 °C using a FEI Vitrobot to maintain a constant humidity environment. A droplet of 2–4 μL of micelle solution was added to a holey carbon-coated copper grid, and the grid was blotted to remove excess solution. The grid was subsequently plunged into liquid ethane to vitrify the sample. Grids were transferred to a Gatan cryo stage and imaged at 120 keV using a Tecnai G2 12 Twin TEM equipped with a Gatan CCD camera. The temperature of the cryo stage was maintained below −170 °C during imaging. Images were analyzed using Gatan DigitalMicrograph software.

Small angle X-ray scattering (SAXS). SAXS data were obtained on the DND-CAT beamline at the Advanced Photon Source (APS). Data were collected for 60 s using an incident beam wavelength of 0.73 Å and a sample-to-detector distance of 4 m, which gave a scattering vector (q) range of 0.007 $Å^{-1} < q <$ 0.2 $Å^{-1}$. The scattering vector modulus (q) is defined as $q = (4\pi/\lambda)\sin(\theta/2)$, where θ is the scattering angle. Micelle sizes were calculated from the first maximum in the scattering curve using the relationship for spherical scatterers $qR = 5.763$, where R is the micelle radius.[37]

Proton nuclear magnetic resonance spectroscopy (^{1}H NMR). Solutions of PB-PEO for ^{1}H NMR experiments in D_2O and THF-d_8 were prepared according to the procedure in Section 2.2. ^{1}H NMR spectra were obtained at 400.1 MHz on a Bruker-DRX400 Spectrometer. 256 scans with a 1 s relaxation delay were collected for each spectrum.

Small angle neutron scattering (SANS). Solutions of PB-PEO and PB-*d*PEO were prepared in D_2O and THF-d_8 according to the procedure in Section 2.2. SANS experiments were performed on the NG-7 30 m SANS instrument at the National Institute of Standards and Technology, Center for Neutron Research (NIST-CNR). An incident wavelength of 6.0 Å with a wavelength divergence (Δλ/λ) of 0.11 was used with sample-to-detector distances of 1.0 m, 4.0 m, and 13.5 m to cover scattering vectors ranging from 0.004 $Å^{-1} < q <$ 0.4 $Å^{-1}$. Raw SANS data were reduced to 1D data in IGOR Pro with reduction procedures provided by NIST.[38]

SANS model fitting. SANS data were fit with a form factor model for spherical block copolymer micelles.[39–42] Four correlation terms were considered: self-correlation of the core, self-correlation of the corona chains, the cross-term between the core and corona chains, and the cross-term of different corona chains,

$$\begin{aligned} P_{micelle}(q) = {} & N_{Agg}^2\beta_{core}^2 A_{core}^2(q) + N_{Agg}\beta_{corona}^2 P_{chain}(q) \\ & + 2N_{Agg}^2\beta_{core}\beta_{corona}A_{core}(q)A_{corona}(q) \\ & + N_{Agg}(N_{Agg}-1)\beta_{corona}^2 A_{corona}^2(q) \end{aligned} \quad (2)$$

where q is the scattering vector, N_{Agg} is the aggregation number, and β_{core} and β_{corona} are the total excess scattering lengths of the core and corona blocks, respectively. The total excess scattering lengths are defined as $\beta_{core} = \upsilon_{core}(\rho_{core} - \rho_{solvent})$ and $\beta_{corona} = \upsilon_{corona}(\rho_{corona} - \rho_{solvent})$, where υ_{core} and υ_{corona} are the volumes of the core and corona blocks, and ρ_{core}, ρ_{corona}, and $\rho_{solvent}$ are the scattering length densities of the core, corona, and cosolvent mixtures, respectively.

The scattering amplitude for a spherical homogeneous core, with radius R_c, is

$$A_{core}(q) = \Phi(qR_c)\exp(-q^2\sigma_{int}^2/2) \quad (3)$$

with $\Phi(x) = 3[\sin x - x\cos x]/x^3$ Here, the exponential term describes a smoothly decaying density profile of width σ_{int} at the core-corona interface.

Self-correlation of the corona chains was approximated by a Debye function,

$$P_{chain}(q) = 2[\exp(-q^2R_g^2) - 1 + q^2R_g^2]/(q^2R_g^2)^2 \quad (4)$$

where the chains were assumed to be Gaussian coils with radius of gyration, R_g.

A radial density distribution of corona chains, $\rho_{corona}(r)$, was considered, and the scattering amplitude was calculated from the normalized Fourier transform of the radial density distribution of corona chains

$$A_{corona}(q) = \frac{4\pi\int\rho_{corona}(r)[\sin(qr)/qr]r^2\,dr}{4\pi\int\rho_{corona}(r)r^2dr}\exp\left(-q^2\sigma_{int}^2/2\right) \quad (5)$$

We represented the corona density profile, $\rho_{corona}(r)$, as a linear combination of two cubic b splines. This explicit form of $\rho_{corona}(r)$ was originally developed by Pedersen and co-workers[42] and has been successfully implemented to describe scattering from micelles in aqueous[39] and organic solutions.[40–42] Furthermore, this density profile model was able to adapt to changes in the corona profile induced by cosolvent addition because it independently fit the width of the corona profile and the linear combination of 2 cubic b splines.

We also incorporated a Schulz distribution of core radii into the model to account for polydispersity in micelle size[43]

$$G(R_c) = \frac{R_c^Z}{\Gamma(Z+1)}\left(\frac{Z+1}{\langle R_c\rangle}\right)^{Z+1}\exp[-(Z+1)R_c/\langle R_c\rangle] \quad (6)$$

where $\langle R_c\rangle$ is the average core radius, and Z is related to the polydispersity, σ_{Rc}, by $\sigma_{Rc}^2 = 1/(Z+1)$. The coherent scattered intensity for the polydisperse micelle model was then given by

$$I(q) = \int P_{micelle}(q)G(R_c)dR_c \quad (7)$$

Because intermicellar interactions were negligible at the solution concentrations used in our studies,[25] scattering contributions from a structure factor were not included in the model. The calculated scattering intensity was further corrected for instrument resolution by employing procedures provided by NIST.[38]

3. Results

To investigate the effects of interfacial tension on PB-PEO micelle assemblies, we used contact angle measurements on PB

thin films to determine the interfacial tension between PB and H_2O/THF mixtures. As seen in Fig. 1, the PB-cosolvent interfacial tension decreased with increasing THF content from ~50 mN m^{-1} in pure water to ~5 mN m^{-1} in 70 vol% THF. Thus, the THF content in the cosolvent mixture could tune the core-corona interfacial tension over approximately one order of magnitude in PB-PEO micelles.

PB-PEO micelle solutions in H_2O/THF mixtures (0–60 vol% THF) were analyzed by DLS, SAXS, and cryo-TEM to determine micelle hydrodynamic radius, R_h, (DLS), micelle outer radius, R_m, (SAXS), and micelle core radius, R_c, (cryo-TEM) as a function of THF content [Fig. 2, Table 1, and Supplementary Information Fig. S1]. Angle dependent DLS measurements indicated that the micelles remained spherical upon THF addition [Supplementary Information, Fig. S1].[44] The data in Fig. 2(a) show that R_h, R_m, and R_c decreased with THF addition due to the reduction in interfacial tension, consistent with previously reported experimental studies.[6,18,19]

Comparing R_c with the corona thickness, H, defined as $H = R_m$-R_c, we see that $H > R_c$ over the range of THF contents, suggesting that the micelles were starlike [Table 1].[8,20] According to theoretical scaling relationships for starlike micelles,[8] R_c should scale with interfacial tension, γ, as $R_c \sim \gamma^{2/5}$ and with H as $H \sim \gamma^{6/25}$. Using the experimentally determined interfacial tensions, these scaling laws were fit to the measured core and micelle radii. As seen in Fig. 2(a), the experimental data were in good agreement with these theoretical scaling relationships.

To further elucidate changes in the micelle structure induced by cosolvent mixtures, we performed contrast variation SANS experiments. The contrast variation between PB-PEO and PB-*d*PEO allowed in-depth examination of the micelle structural profile through simultaneous fitting of the form factor model for block copolymer micelles to the complementary deuterated and non-deuterated data sets. Minor discrepancies were noted between the PB-PEO and PB-*d*PEO micelles due to the slight difference in polymer molecular weights. These differences were considered when simultaneously fitting the data such that the differences in fit parameters for core radius, R_c, and aggregation number, N_{Agg}, were consistent with the small discrepancy in polymer molecular weight. Cosolvent effects on the core size and core-corona interfacial width, σ_{int}, (*i.e.* where the core and corona blocks were mixed) were determined by fitting the PB-*d*PEO data, while changes in the overall micelle size and corona density profile were found by fitting the PB-PEO data.

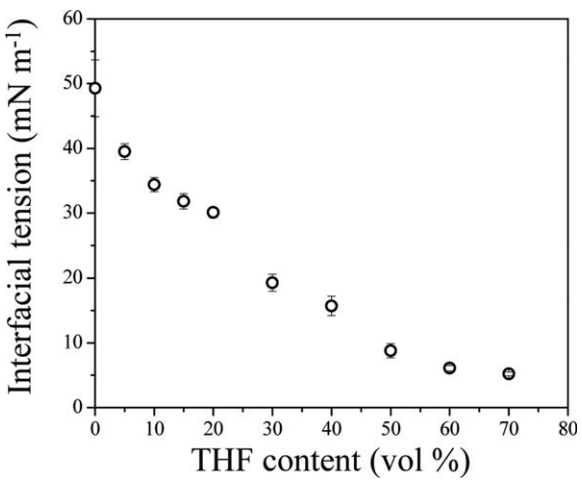

Fig. 1 PB-cosolvent interfacial tension as a function of THF content. Error bars represent the range of calculated values due to variability in contact angle measurements.

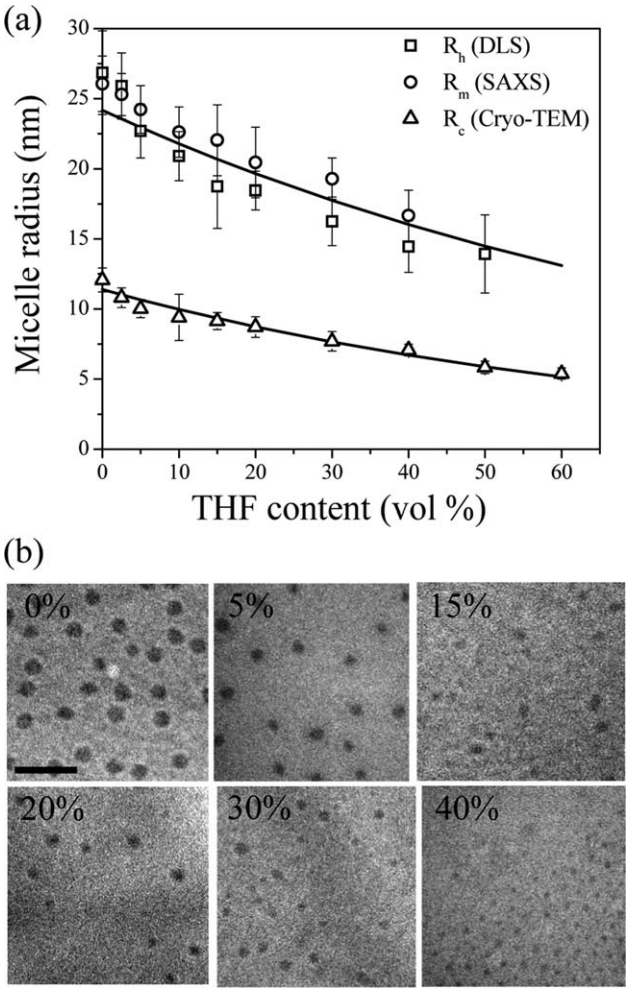

Fig. 2 (a) DLS, SAXS, and cryo-TEM data showing the micelle hydrodynamic radius R_h, micelle outer radius R_m, and micelle core radius R_c, *vs.* THF content in H_2O/THF mixtures. Solid lines are the theoretical predications of R_c and R_m for starlike micelles in a good solvent. Error bars represent the range in measured radii. (b) Cryo-TEM micrographs of PB-PEO micelles in H_2O/THF mixtures at 0, 5, 15, 20, 30, and 40 vol% THF (scale bar = 100 nm). Note that only the PB cores are visible in the micrographs due to minimal electron density contrast between PEO and water.

Quality fits for the PB-PEO and PB-*d*PEO SANS data up to 40 vol% THF-d_8 were obtained by using only the micelle form factor model [Fig. 3]. However, at higher THF-d_8 contents, the presence of free chains in solution affected the scattering at high q.[45] To account for the free chains in solution, the SANS data (40 vol% to 72 vol%) were fit to a linear combination of spherical micelle and Gaussian coil form factors.[46] By enforcing a constant polymer solution concentration, the fraction of free polymer chains was estimated from the relative scaling of the two models. These combined SANS fits suggested that the fraction of free chains increased with THF-d_8 content up to 72 vol% THF-d_8 [Table 1],

Table 1 Micelle composition data determined by DLS, SAXS, cryo-TEM, and SANS, where N_{Agg} is micelle aggregation number, R_c is core radius, σ_{Rc} is core polydispersity, σ_{int} is interfacial width, R_h is hydrodynamic radius, R_m is micelle radius, H is the corona thickness, where $H = R_m - R_c$ estimated from R_m (SAXS) and R_c (cryo-TEM), and R_g is radius of gyration of PEO corona chains

Solvent composition (vol% THF)	N_{Agg} SANS	Fraction of free chains SANS	R_c (nm) Cryo-TEM	R_c (nm) SANS	σ_{Rc} (nm) SANS	σ_{int} (nm) SANS	R_h (nm) DLS	R_m (nm) SAXS	R_m[a] (nm) SANS	H (nm) SAXS/ Cryo-TEM	PEO R_g (nm) SANS
0.0	791 ± 1	—	12.1 ± 0.9	11.2 ± 0.1	0.05	0.11 ± 0.09	26.9 ± 3.0	26.1 ± 2.0	27.8 ± 0.1	14.0 ± 2.2	3.7 ± 0.1
2.5	—	—	10.8 ± 0.7	11.2 ± 0.1	0.08	0.10 ± 0.10	25.9 ± 2.4	25.3 ± 1.5	—	14.5 ± 1.7	—
5.0	598 ± 1	—	10.0 ± 0.7	10.8 ± 0.1	0.12	0.10 ± 0.10	22.7 ± 1.9	24.2 ± 1.7	26.7 ± 0.1	14.2 ± 1.8	4.1 ± 0.2
10.0	419 ± 1	—	9.4 ± 1.7	9.3 ± 0.1	0.10	0.15 ± 0.15	20.9 ± 1.8	22.6 ± 1.8	24.4 ± 0.1	13.2 ± 2.5	4.0 ± 0.3
15.0	326 ± 1	—	9.2 ± 0.6	9.1 ± 0.1	0.15	0.15 ± 0.05	18.8 ± 3.0	22.0 ± 2.5	23.2 ± 0.1	12.8 ± 2.6	4.0 ± 0.1
20.0	248 ± 1	—	8.7 ± 0.7	8.6 ± 0.1	0.18	0.15 ± 0.05	18.5 ± 1.4	20.4 ± 2.5	21.9 ± 0.1	11.7 ± 2.6	4.1 ± 0.3
30.0	143 ± 1	—	7.7 ± 0.7	7.7 ± 0.1	0.18	0.15 ± 0.15	16.3 ± 1.7	19.3 ± 1.5	18.6 ± 0.1	11.6 ± 1.7	3.8 ± 0.1
40.0	88 ± 5	0.08 ± 0.02	7.1 ± 0.4	6.7 ± 0.1	0.18	0.89 ± 0.79	14.5 ± 1.8	16.7 ± 1.8	16.1 ± 0.2	9.6 ± 1.8	3.5 ± 0.4
50.0	67 ± 5	0.10 ± 0.02	5.8 ± 0.4	6.0 ± 0.3	0.18	1.00 ± 0.50	13.9 ± 2.8	—	14.8 ± 0.4	—	3.6 ± 0.1
60.0	60 ± 11	0.26 ± 0.09	5.4 ± 0.4	5.3 ± 1.1	0.18	1.28 ± 1.08	—	—	13.5 ± 1.2	—	2.4 ± 0.3
70.0	52 ± 19	0.48 ± 0.30	—	3.8 ± 1.5	0.20	2.18 ± 0.54	—	—	12.7 ± 1.5	—	1.6 ± 0.2
72.0	30 ± 5	0.90 ± 0.18	—	4.4 ± 1.2	0.20	2.31 ± 0.51	—	—	11.6 ± 0.8	—	1.5 ± 0.1

[a] R_m from SANS estimated based on corona density profile where the volume fraction of PEO < 0.02.[39]

at which point the micelles disassembled. We note that separate turbidity measurements on solutions of our parent PB homopolymer indicated that PB was fully soluble in H_2O/THF mixtures containing above ~75 vol% THF [Supplementary Information, Fig. S2], consistent with the micelle disassembly threshold suggested by the SANS data modeling.

The SANS data fits describing the effects of cosolvent composition on micelle structure are shown in Fig. 4, Fig. 5, and Table 1. A decrease in R_m and R_c [Fig. 4(a) and Table 1] with increasing THF-d_8 content was found, consistent with the DLS, SAXS, and cryo-TEM data [Fig. 2(a) and Table 1]. Here, we defined R_m as the radius at which the volume fraction of PEO was less than 0.02 in the corona profile [Fig. 5].[39] The decrease in R_m and R_c also followed the trend of reduced N_{Agg} as THF-d_8 was added [Fig. 4(b), and Table 1]. While the micelle size decreased with THF-d_8 addition, the polydispersity in micelle sizes increased. This increased polydispersity can be seen qualitatively in the smearing of the first minimum and maximum in the SANS data [Fig. 3] and was quantified by the SANS data modeling, which gave reasonable size distributions.

The SANS models also allowed characterization of cosolvent effects on the micelle composition profile. In pure D_2O, the characteristic sharp interface between the PB core and PEO corona was shown by the negligible σ_{int} value, and this sharp profile persisted up to ~30 vol% THF-d_8 [Fig. 4(a) and Table 1]. However, as more THF-d_8 was added (>30 vol% THF-d_8), σ_{int} increased, signifying the mixing of PB and PEO at the core-corona interface, and consequently, the broadening of that interface. Also, as THF-d_8 was added, the solvent fraction in the core increased, indicating that the micelle cores were swelling with solvent [Fig. 4(b)]. The solvent fraction in the core was calculated using the fit values for N_{Agg} and R_c, and was not calculated for samples containing >30 vol% THF-d_8 due to the lack of a well-defined core size.

The changing solvent conditions also affected the micelle corona profile. A rescaled corona composition, $\hat{\rho}_{corona}(r)$, was calculated by normalizing the corona density profile obtained from the SANS data fitting, $\rho_{corona}(r)$, to the total volume of the corona (PEO plus solvent),[40]

$$\int 4\pi \hat{\rho}_{corona}(r) r^2 dr = N_{Agg} \upsilon_{corona} \tag{8}$$

Profiles for $\hat{\rho}_{corona}$ *versus* r are presented in Fig. 5. As seen in the figure, the maximum volume fraction of PEO at the core-corona interface, along with the total PEO content in the micelle corona, decreased with reducing interfacial tension, reflecting the improved solvent quality for the core block and the reduction in N_{Agg}.[40] The corona brush thickness also decreased with increasing THF-d_8 content, reflecting the changing curvature of the micelle core surface.

To investigate the effects of THF addition on the solvent quality for PEO, we performed SANS experiments on PEO homopolymer (M_n = 6.3 kg mol^{-1}) in D_2O/THF-d_8 mixtures ranging from 0–70 vol% THF [Supplementary Information, Fig. S3]. The SANS data were fit with a Debye function to determine changes in the radius of gyration, R_g, as a function of THF-d_8 content.[46] These data confirmed that the changing solvent conditions had little effect on the PEO R_g, similar to the small changes in the micelle corona up to 60 vol% THF-d_8, as

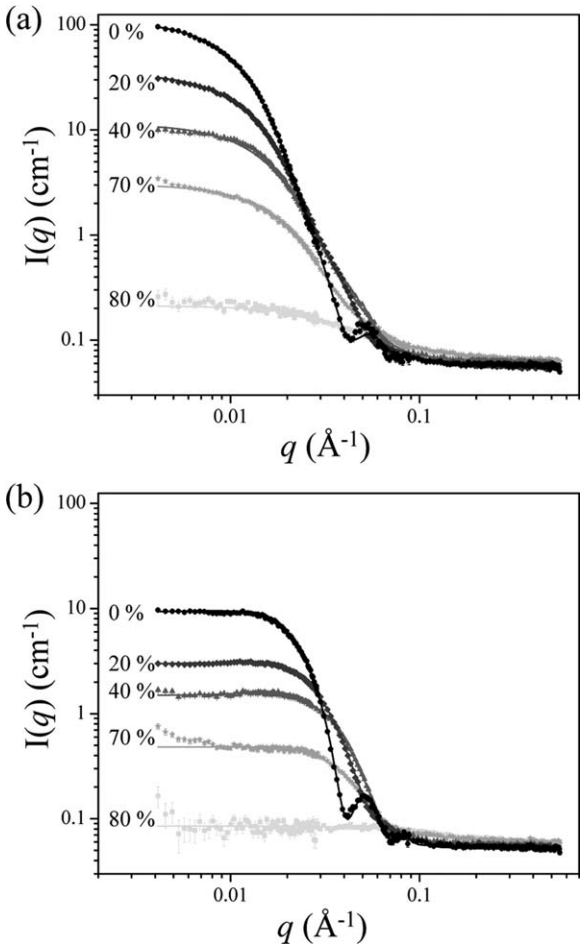

Fig. 3 SANS data (symbols) and fits (solid lines) for PB-PEO (a) and PB-*d*PEO (b) in D_2O/THF-d_8 mixtures, where labels indicate the volume percent of THF-d_8 in the cosolvent mixture. Error bars represent the standard deviation in the measured intensity.

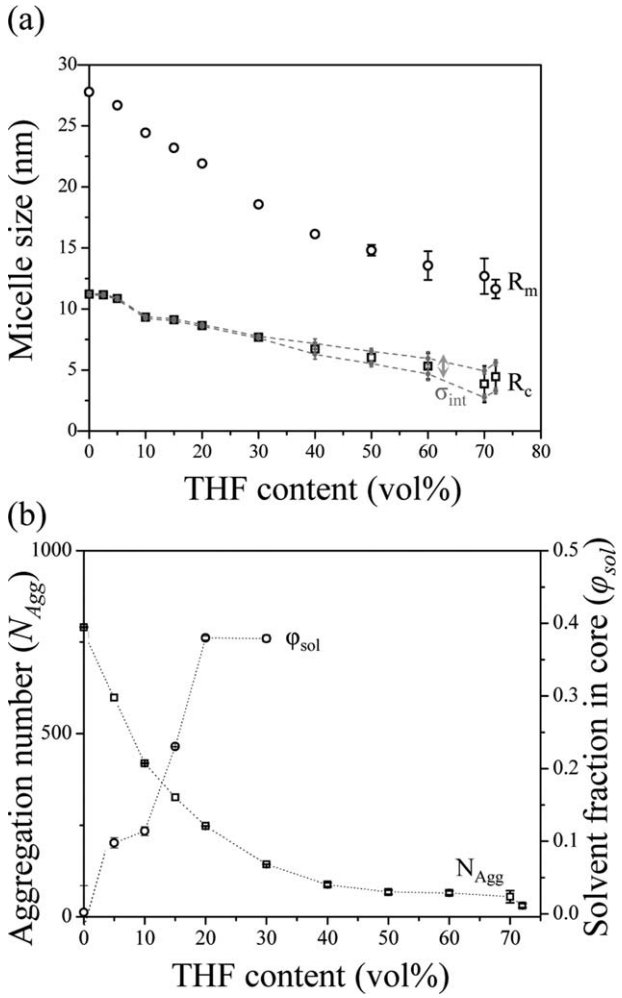

Fig. 4 Composition changes in PB-PEO/PB-*d*PEO micelles in D_2O/THF-d_8 mixtures determined from SANS data fitting. Error bars for R_c, R_m, σ_{int}, and N_{Agg}, represent the range of fit values with similar goodness of fits; error bars for φ_{sol} represent the range of calculated values due to uncertainty in the fit parameters used in the calculation.

determined from SANS modeling [Table 1]. While a significant decrease in R_g in the micelle corona was noted for >60 vol% THF-d_8, these fit values for PEO R_g were unreliable because the high q scattering in these solutions was dominated by free chains.

The SANS studies presented above were complemented by ^{1}H NMR experiments to probe PB chain mobility at various THF-d_8 contents [Fig. 6]. In pure THF-d_8, the polymer was fully solvated, and peaks corresponding to both PB (between 0.8–2.1 ppm and 4.8–5.6 ppm) and PEO (3.6 ppm) were detected by ^{1}H NMR. In contrast, in pure D_2O, only the peak corresponding to the PEO corona was detected. Because D_2O was a non-solvent for the PB, the PB chains were confined to the micelle core in pure D_2O, and the restricted chain motion led to broad and weak PB peaks. As THF-d_8 was added to the system, the PB mobility increased, as manifested by a sharpening of the corresponding peaks [Fig. 6(a)].[47] The fraction of mobile PB was quantified by comparing the integrated PB peak areas in micelle solutions at various THF-d_8 contents to PB peak areas in pure THF-d_8, where the block copolymer was fully solvated. Fig. 6(b) shows that the PB mobility increased with THF-d_8 content up to ~50 vol% THF-d_8, at which point the PB had similar mobility to fully solvated chains. This increased PB mobility indicated that the

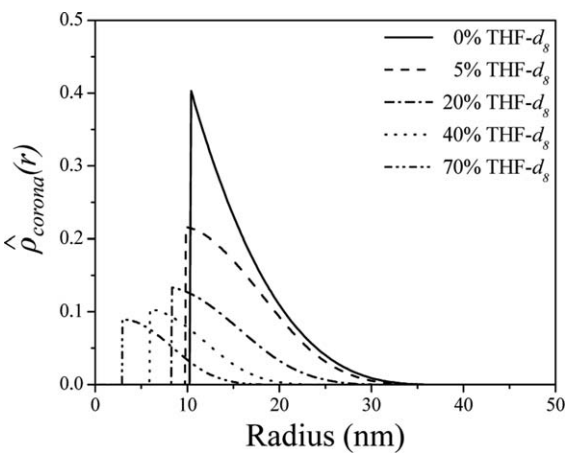

Fig. 5 Radial composition profile in PEO corona in PB-PEO micelles in D_2O/THF-d_8 mixtures as determined from SANS data fitting.

core was swelling with THF-d_8 [Fig. 4(b)] and that PB chains were likely solvated and being expressed outside of a well-defined micelle core. Above 50 vol% THF-d_8, the PB peaks continued to sharpen, implying that the polymer chains were becoming more mobile. The continued increase in chain mobility shown by ^{1}H NMR was consistent with a mixture of free chains and micelles, in agreement with our SANS analysis [Table 1].

4. Discussion

We have demonstrated control over the micellization properties of PB-PEO by using cosolvent mixtures to manipulate the core-corona interfacial tension. The combination of real space and Fourier space techniques in the analysis of PB-PEO micelles led to new insights into the changes in micelle structure as a function of interfacial tension. The micelle sizes obtained by DLS, SAXS, and cryo-TEM data [Fig. 2(a) and Table 1] agreed well with the values obtained from SANS data fitting [Fig. 4(a) and Table 1]. These data sets from multiple analytical techniques showed a decrease in micelle size as the interfacial tension was reduced. The lowered interfacial tension led to an increased core chain interfacial area, which favored the formation of smaller micelles with lower aggregation numbers.

The combination of analytical techniques also allowed detailed characterization of the effects of THF addition on the micelle core size, R_c. While previous studies showed a decrease in overall micelle size with reduced interfacial tension, these studies did not independently measure the micelle core size.[6,19] Instead, they calculated the core size based on the measured aggregation number, and they assumed either that there was no solvent in the core[6] or that the solvent fraction in the core was equal to the volume fraction of organic cosolvent in the micelle solution.[19] Our experimental measurements of both the core size and aggregation number show that solvent was indeed present in the core and that the solvent fraction in the core was greater than the volume fraction of THF in the cosolvent mixture [Fig. 4(b)], in contrast to previous assumptions. We have shown that cosolvent addition not only leads to a decrease in R_c, but an increase in the solvent fraction in the core [Fig. 4(b)].

In addition to R_c, the corona thickness, H, decreased as the THF content increased [Fig. 2, Fig. 4(a), and Table 1], where H decreased from ~18 nm to ~10 nm over the THF content range used in this study. For the PEO corona chains ($N = 183$), the theoretical root-mean-square end-to-end distance, r_e, is 9.1 nm.[39] Thus, $H > r_e$ at all THF contents, suggesting that the corona chains were stretched, consistent with the definition of starlike micelles.[8,20] The starlike profile also was evident in the good fits of our SANS data, where we used a form factor model that accounted for a radial density distribution of corona chains. Furthermore, comparing the core and corona dimensions showed that $H > R_c$ throughout the range of solvent compositions, characteristic of a starlike structure. Likewise, comparing our experimental results to theoretical scaling relationships for starlike micelles showed an excellent correlation between experiment and theory for changes in R_c and H with decreasing core-corona interfacial tension [Fig. 2(a)]. The agreement between our experimental results and scaling theory suggested that the decrease in R_c and H was primarily due to the change in interfacial tension induced by solvent addition, and reflected the

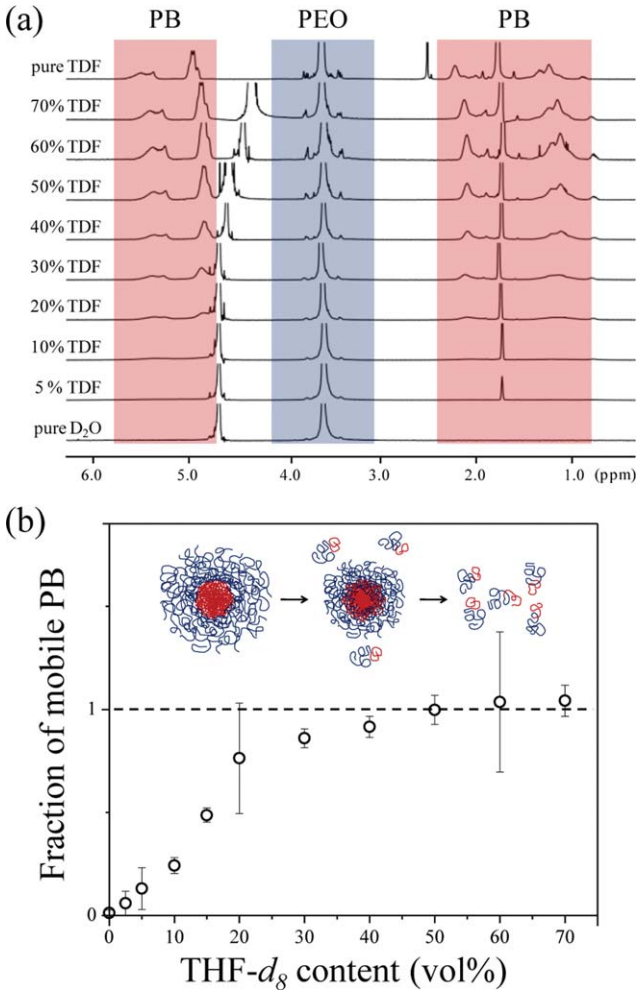

Fig. 6 (a) ^{1}H NMR spectra of PB-PEO micelles in D_2O/THF-d_8 mixtures, where boxed regions highlight the peaks associated with PB and PEO blocks. (b) Fraction of mobile PB chains in PB-PEO micelles calculated from (a). Error bars in (b) represent standard deviation in values from three experimental trials. Inset in (b): cartoon representation of the changes in micelle structure with increasing THF content.

increase in curvature at the core surface as the micelle size decreased. This result was supported by the small change in the PEO R_g for both the corona chains [Table 1] and the PEO homopolymer [Supplementary Information Fig. S3] with THF addition, which suggested that the changing solvent conditions had very little effect on the PEO chain dimensions. Thus, the use of H_2O/THF mixtures led to control of the micelle core size and the corona thickness, all with a single block copolymer.

The decrease in interfacial tension also affected the composition profile at the micelle core-corona interface, as determined using contrast variation SANS experiments. Because scattering contributions from the corona were minimized, our SANS model fits for the PB-*d*PEO data were sensitive to the core-corona interfacial width (σ_{int} in the model). In pure D_2O, the micelles had a sharp core-corona interface due to the highly amphiphilic nature of PB-PEO.[11,25–27] As the THF-d_8 content increased, the core-corona interface became more diffuse due to the reduction in interfacial tension, resulting in broader interfaces at >30 vol% THF-d_8. The effects of interfacial tension on polymer interfaces

have been well studied for bulk systems, such as homopolymer blends and block copolymers.[21–24] Here we have shown that interfacial tension also controlled the core-corona interfacial width in solution assemblies, as illustrated in Fig. 4(a), where a broad core-corona interfacial width was seen in PB-PEO micelles at higher THF-d_8 contents (*i.e.* lower core-corona interfacial tensions).

The broadening of the interfacial width evident from the SANS data [Fig. 4(a) and Table 1] for the samples containing higher THF-d_8 contents was an exciting feature in these structures. The PB chains at the interface became solvent accessible as the THF content was increased, giving rise to two distinct PB regions in the micelle: hidden chains in the core, and accessible chains at the core-corona interface. The exposed PB chains at the interface should enable micelle corona functionalization in future experiments.

In addition to the broadening of the core-corona interface, the reduced interfacial tension resulted in a lower PEO volume fraction at the core surface [Fig. 5]. In pure D_2O, there was a high volume fraction of PEO at the core-corona interface, implying that a collapsed layer of PEO surrounded the micelle core to minimize the unfavorable PB-water interactions, consistent with previous studies.[25,48] As the interfacial tension decreased with THF-d_8 addition, the maximum volume fraction of PEO at the core-corona interface decreased, because less shielding of the PB chains was necessary.

Adding THF to the PB-PEO solutions also affected the concentration of free polymer chains in solution. In pure water, the concentration of free chains was negligible due to the extremely low critical aggregation concentration (CAC), which is reported to be on the order of 10^{-6} g mL^{-1} for comparable molecular weight PB-PEO block copolymers in water.[49,50] However, examination of the high q scattering in the SANS data indicated that a significant concentration of free chains was present as the THF-d_8 content increased to >30 vol% [Table 1]. By fitting the SANS data for >30 vol% THF-d_8 with a combined form factor model for micelles and Gaussian chains, we determined that the concentration of free chains increased with added THF-d_8 until complete micelle disassembly. The presence of free chains in solution was corroborated by ^{1}H NMR studies that showed increased PB mobility at higher THF-d_8 contents. This coexistence of free chains and micelles was possibly due to an increase in the CAC, resulting from the reduced interfacial tension caused by THF addition.[51–53] Assuming the maximum concentration of free chains in solution was equal to the CAC, we saw an exponential increase in the CAC with decreasing interfacial tension, which was in accordance with micelle formation theory.[51,54] We note that free chains were possibly present in solution at THF contents lower than 30 vol%; however, the SANS data modeling was not sensitive to the low concentration of chains at these THF fractions. One circumstantial indicator of free chains at lower THF contents can be found in the interfacial tension results in Fig. 1, where a noticeable discontinuity in the data between 20 and 30 vol% THF could possibly indicate a sharp change in interfacial tension behavior.

Another effect of high THF-d_8 contents (>50 vol%) shown in the SANS data [Fig. 3] was an upturn in intensity at low q values. This upturn became more pronounced as the THF-d_8 content was increased and suggested the presence of larger structures in solution. Previous studies by Dewalt *et al.* reported PS-PEO micelle aggregation in H_2O/THF mixtures at THF contents >50 vol%.[18] Hence, we speculate that the increased low q scattering could be due to the aggregation of micelles beginning at >50 vol% THF.

5. Conclusions

We have manipulated the structure of PB-PEO micelles in aqueous solutions by adding THF as a cosolvent to reduce the core-corona interfacial tension. Overall, we have demonstrated excellent control over the micelle size, including both core size and corona thickness, through the addition of cosolvents to a single block copolymer. This method eliminates the need for the synthesis of multiple block copolymers to achieve the same range of micelle sizes.

We have shown excellent agreement between our experimental results and theoretical models of starlike micelles for the dependence of core size and corona thickness on interfacial tension. Changes in the internal micelle structure were elucidated by performing contrast variation SANS experiments. The incorporation of both micelle and Gaussian coil form factors in our SANS models facilitated data fitting at high THF contents, where a significant number of free chains in solution were evident. Also, by minimizing scattering contributions from the micelle corona (using PB-*d*PEO), we characterized the core-corona interfacial region and demonstrated that lowering the core-corona interfacial tension led to broader core-corona interfaces. The broadening of polymer interfacial profiles with decreasing interfacial tension has been shown for polymers in the bulk, and here we have demonstrated that interfacial tension also controls the core-corona interfacial width in solution assemblies. We also note that the micelle cores swelled with THF addition, and that the solvent fraction in the core was greater than the volume fraction of THF cosolvent mixture, suggesting that previous assumptions regarding the micelle core solvent content in cosolvent mixtures may not be accurate. The broader core-corona interface, swollen core, and lower PEO volume fraction at the core surface rendered the PB chains more solvent accessible at high THF contents.

The use of a cross-linkable core block (as is the case here) will allow these solvent induced structures to be fixed in future experiments, enabling the removal of THF and the subsequent use of the micelles in biomedical applications. The combination of PB core chains in a solvent poor environment, and solvent accessible PB chains at the core-corona interface is an important feature. The two distinct PB environments will permit partial cross-linking using the core PB chains to fix the structures, while leaving the remaining interfacial PB chains available for functionalizing the micelles. In future studies, we will utilize the pendant vinyl bonds of the solvent accessible PB chains to stabilize these solvent induced structures by partial cross-linking, and will functionalize the cross-linked micelles with biologically relevant ligands. Control over the size, corona thickness, and extent of solvent accessible PB in these micelles will be a powerful tool in the development of targeting delivery vehicles.

Acknowledgements

This work was supported by NIH-NCRR COBRE (#P20RR017716) and NIST, U.S. Department of Commerce

(#70NANB7H6178). The statements herein do not reflect the views of NIH. E.G.K. was supported by a DoD NDSEG Fellowship. Certain commercial equipment, instruments, materials, suppliers and software are identified in the paper to aid understanding. Such identification does not imply recommendation or endorsement by the National Institute of Standards and Technology, nor does it imply that the materials or equipment identified are necessarily the best available for the purpose. SAXS data were collected at the DND-CAT, Sector 5 of the Advanced Photon Source (APS). DND-CAT is supported by E. I. DuPont de Nemours & Co., The Dow Chemical Company, and the State of Illinois. Use of the APS was supported by the DoE, Office of Science, BES (#DE-AC02-06CH11357). ^{1}H NMR spectra were collected on instrumentation supported by NSF CRIF: MU CEH 0840401. We acknowledge the Keck Microscopy Facility for use of their TEM and Vitrobot, and the Center for Molecular and Engineering Thermodynamics for use of their DLS. We thank Dr Y. Liu, Dr P. Butler, and Dr J. Seppala for helpful SANS discussions. We also thank Prof. J. O'Donnell for assistance with polymer characterization, Ms. J. Albert for assistance with contact angle measurements, and Ms. C. Marino for contributions to data collection.

References

1 M. L. Adams, A. Lavasanifar and G. S. Kwon, *J. Pharm. Sci.*, 2003, **92**, 1343–1355.
2 J. A. Zupancich, F. S. Bates and M. A. Hillmyer, *Biomacromolecules*, 2009, **10**, 1554–1563.
3 Y. Geng, D. E. Discher, J. Justynska and H. Schlaad, *Angew. Chem., Int. Ed.*, 2006, **45**, 7578–7581.
4 X. Huang, X. Peng, Y. Wang, D. M. Shin, M. A. El-Sayed and S. Nie, *ACS Nano*, 2010, **4**, 5887–5896.
5 J. N. Israelachvili, D. J. Mitchell and B. W. Ninham, *Journal of the Chemical Society, Faraday Transactions 2: Molecular and Chemical Physics*, 1976, **72**, 1525–1568.
6 R. Lund, L. Willner, J. Stellbrink, A. Radulescu and D. Richter, *Macromolecules*, 2004, **37**, 9984–9993.
7 R. Lund, V. Pipich, L. Willner, A. Radulescu, J. Colmenero and D. Richter, *Soft Matter*, 2011, **7**, 1491–1500.
8 A. Halperin, M. Tirrell and T. P. Lodge, *Adv. Polym. Sci.*, 1992, **100**, 31–71.
9 A. Blanazs, S. P. Armes and A. J. Ryan, *Macromol. Rapid Commun.*, 2009, **30**, 267–277.
10 T. Smart, H. Lomas, M. Massignani, M. V. Flores-Merino, L. R. Perez and G. Battaglia, *Nano Today*, 2008, **3**, 38–46.
11 S. Jain and F. S. Bates, *Science*, 2003, **300**, 460–464.
12 C. Fernyhough, A. J. Ryan and G. Battaglia, *Soft Matter*, 2009, **5**, 1674–1682.
13 J. P. A. Fairclough, A. I. Norman, B. Shaw, V. M. Nace and R. K. Heenan, *Polym. Int.*, 2006, **55**, 793–797.
14 H. Shen and A. Eisenberg, *J. Phys. Chem. B*, 1999, **103**, 9473–9487.
15 A. Choucair and A. Eisenberg, *Eur. Phys. J. E*, 2003, **10**, 37–44.
16 A. Choucair, C. Lavigueur and A. Eisenberg, *Langmuir*, 2004, **20**, 3894–3900.
17 C. Liu, M. A. Hillmyer and T. P. Lodge, *Langmuir*, 2008, **24**, 12001–12009.
18 L. E. Dewalt, H. D. Ou-Yang and V. L. Dimonie, *J. Appl. Polym. Sci.*, 1995, **58**, 265–269.
19 Y. S. Seo, M. W. Kim, D. H. Ou-Yang and D. G. Peiffer, *Polymer*, 2002, **43**, 5629–5638.
20 A. Halperin, *Macromolecules*, 1987, **20**, 2943–2946.
21 E. Helfand and Y. Tagami, *J. Polym. Sci., Part B: Polym. Lett.*, 1971, **9**, 741–746.
22 E. Helfand and Y. Tagami, *J. Chem. Phys.*, 1972, **56**, 3592–3601.
23 E. Helfand and A. M. Sapse, *J. Chem. Phys.*, 1975, **62**, 1327–1331.
24 A. N. Semenov, *Macromolecules*, 1993, **26**, 6617–6621.
25 Y. Y. Won, H. T. Davis, F. S. Bates, M. Agamalian and G. D. Wignall, *J. Phys. Chem. B*, 2000, **104**, 7134–7143.
26 Y. Y. Won, H. T. Davis and F. S. Bates, *Macromolecules*, 2003, **36**, 953–955.
27 S. Jain and F. S. Bates, *Macromolecules*, 2004, **37**, 1511–1523.
28 Y. Y. Won, K. Paso, H. T. Davis and F. S. Bates, *J. Phys. Chem. B*, 2001, **105**, 8302–8311.
29 B. M. Discher, H. Bermudez, D. A. Hammer, D. E. Discher, Y. Y. Won and F. S. Bates, *J. Phys. Chem. B*, 2002, **106**, 2848–2854.
30 M. A. Hillmyer and F. S. Bates, *Macromolecules*, 1996, **29**, 6994–7002.
31 R. P. Quirk, D. L. Gomochak, C. Wesdemiotis and M. A. Arnould, *J. Polym. Sci., Part A: Polym. Chem.*, 2003, **41**, 947–957.
32 C. M. Stafford, K. E. Roskov, T. H. Epps, III and M. J. Fasolka, *Rev. Sci. Instrum.*, 2006, **77**, 0239081–0239087.
33 J. N. L. Albert, M. J. Baney, C. M. Stafford, J. Y. Kelly and T. H. Epps, III, *ACS Nano*, 2009, **3**, 3977–3986.
34 B. B. Sauer and N. V. Dipaolo, *J. Colloid Interface Sci.*, 1991, **144**, 527–537.
35 W. J. Cheong and P. W. Carr, *J. Liq. Chromatogr. Relat. Technol.*, 1987, **10**, 561–581.
36 S. W. Provencher, *Comput. Phys. Commun.*, 1982, **27**, 229–242.
37 R.-J. Roe, *Methods of X-ray and Neutron Scattering in Polymer Science*, Oxford University Press, New York, 2000.
38 S. R. Kline, *J. Appl. Crystallogr.*, 2006, **39**, 895–900.
39 J. S. Pedersen and M. C. Gerstenberg, *Colloids Surf., A*, 2003, **213**, 175–187.
40 J. Bang, K. Viswanathan, T. P. Lodge, M. J. Park and K. Char, *J. Chem. Phys.*, 2004, **121**, 11489–11500.
41 S. Y. Choi, F. S. Bates and T. P. Lodge, *J. Phys. Chem. B*, 2009, **113**, 13840–13848.
42 J. S. Pedersen, C. Svaneborg, K. Almdal, I. W. Hamley and R. N. Young, *Macromolecules*, 2003, **36**, 416–433.
43 P. Bartlett and R. H. Ottewill, *J. Chem. Phys.*, 1992, **96**, 3306–3318.
44 R. L. Xu, M. A. Winnik, F. R. Hallett, G. Riess and M. D. Croucher, *Macromolecules*, 1991, **24**, 87–93.
45 N. Willet, J. F. Gohy, L. Auvray, S. Varshney, R. Jérôme and B. Leyh, *Langmuir*, 2008, **24**, 3009–3015.
46 J. S. Higgins and H. C. Benoît, *Polymers and Neutron Scattering*, Oxford Science Pubblications, Oxford, 1996.
47 J. Kriz, B. Masar, H. Pospisil, J. Plestil, Z. Tuzar and M. A. Kiselev, *Macromolecules*, 1996, **29**, 7853–7858.
48 T. P. Smart, O. O. Mykhaylyk, A. J. Ryan and G. Battaglia, *Soft Matter*, 2009, **5**, 3607–3610.
49 Y. Y. Won, A. K. Brannan, H. T. Davis and F. S. Bates, *J. Phys. Chem. B*, 2002, **106**, 3354–3364.
50 S. Pispas and N. Hadjichristidis, *Langmuir*, 2002, **19**, 48–54.
51 J. N. Israelachvili, *Intermolecular & Surface Forces*, 9th edn, Elsevier Science Imprint, London, 2002.
52 Y. S. Yu, L. F. Zhang and A. Eisenberg, *Macromolecules*, 1998, **31**, 1144–1154.
53 L. F. Zhang and A. Eisenberg, *Science*, 1995, **268**, 1728–1731.
54 L. Leibler, H. Orland and J. C. Wheeler, *J. Chem. Phys.*, 1983, **79**, 3550–3557.

